Mixed probabilistic seismic demand models for fragility assessment

Akrivi Chatzidaki[1], Dimitrios Vamvatsikos[1]

[1] Institute of Steel Structures, School of Civil Engineering, National Technical University of Athens, 9 Iroon Polytechneiou str., Zografou Campus, GR-15780 Athens, Greece

Corresponding Author: email: cakrivi@central.ntua.gr

ABSTRACT

A mixture model approach is presented for combining the results of different models or analysis methods into a single probabilistic demand model for seismic assessment. In general, a structure can be represented using models of different type or different number of degrees of freedom, each offering a distinct compromise in computational load versus accuracy; it may also be analysed via methods of different complexity, most notably static versus dynamic nonlinear approaches. Employing the highest fidelity options is theoretically desirable but practically infeasible, at best limiting their use to calibrating or validating lower fidelity approaches. Instead, a large sample of low fidelity results can be selectively combined with sparse results from higher fidelity models or methods to simultaneously capitalize on the frugal nature of the former and the low bias of the latter to deliver fidelity at an acceptable cost. By employing a minimal 5 parameter power-law-based surrogate model we offer two options for forming mixed probabilistic seismic demand models that (i) can combine different models with varying degree of fidelity at different ranges of structural response, or (ii) nonlinear static and dynamic results into a single output suitable for fragility assessment.

KEYWORDS

Probabilistic seismic demand models, multiple fidelity, performance assessment, weighted regression

1 Introduction

Seismic performance assessment lacks no breadth in the choices that an analyst needs to make when tackling any single structure. Structural models can range from minimalistic oscillators to high-resolution behemoths of millions of degrees-of-freedom, each offering different levels of accuracy (e.g. Lachanas and Vamvatsikos, 2020, Silva et al. 2019, Chi et al. 1998). Further issues of the explicit simulation of brittle or ductile failure mechanisms and material/section/member models (e.g. Jalayer et al. 2010, Vamvatsikos and Fragiadakis 2010, Ibarra and Krawinkler 2011, Kazantzi et al. 2014) provide a myriad of options that come with obvious improvements in the fidelity of the results, together with an equally obvious cost in computational resources. Selecting the proper combination of model options is a problem that heavily depends upon the experience of the analyst, the task at hand, and the available resources, namely time, data and computer power.

The typical approach is to select the model and analysis method, accept the consequences and just go with it. Still, there are advantages in being able to combine models and approaches of different fidelity and complexity to deliver a better compromise. Low-fidelity models can be leveraged for achieving speedup at the cost of reduced accuracy, effectively offsetting (and contrasting) the high-expense/high-accuracy of high-fidelity models. Multifidelity approaches can combine low and high-fidelity outputs to achieve an overall improved accuracy in the structural estimate at a reasonable cost, for a final result that is more than the sum of its parts. In the literature, multiple strategies are offered for employing mutlifidelity methods (Peherstorfer et al. 2018), such as adapting the computation process of low-fidelity models based on the outputs of high-fidelity ones (adaptation), combining the results of both low- and high-fidelity models *a posteriori* into a single output (fusion), and filtering the results of low-fidelity models to keep only those consistent with higher fidelity computations (filtering).

In seismic assessment, there are cases where two different model types are complementary, offering improved accuracy at different regions of response. This is the case of distributed plasticity fiber models that offer higher fidelity at low (pre-capping) deformations, while lumped plasticity models are more reliable for larger (post-capping) deformations closer to collapse (Haselton et al., 2007). Combining the two could leverage the complementary benefits of both to deliver a single response model of high fidelity at all deformation/intensity ranges. There are also cases where one approach is clearly the better, but (per the “no free lunch” theorem) also the disproportionally more expensive one, such as the case of nonlinear static versus dynamic analysis (e.g. Fragiadakis et al. 2014). A static procedure can inexpensively provide intensity versus deformation results at all ranges of response, but with non-negligible bias as one deviates from simple first-mode-dominated structures (Krawinkler and Seneviratna 1998). Nonlinear response history analyses (NRHA), suffers from little to no bias (assuming a good structural model), but it is often prohibitively expensive for practical applications. Optimally, a static pushover (SPO) based approach could be relied upon to provide the bulk of the data, while a few higher fidelity dynamic runs could be employed for correcting the bias, e.g., due to higher modes unaccounted for by the SPO.

Overall, in terms of Peherstorfer et al. (2018), we aim to follow a fusion approach to combine via data fitting low- and high-fidelity outputs from distinct structural model and analysis pairs into a single multifidelity surrogate model (Fernández-Godino et al. 2019) of seismic demand. This provides the functional relationship between the input variable, i.e., the intensity measure (IM), and the output of interest, i.e., the Engineering Demand Parameter (EDP) per the Cornell and Krawinkler (2000) performance-based earthquake engineering framework. In the following we aim to describe the conceptual approach to deriving and employing such mixed fidelity models while offering two practical examples of application for the assessment of a 4-story reinforced concrete (RC) frame (i) using lumped and distributed plasticity models and (ii) combining nonlinear static with dynamic analysis.

Mixing demand models

Multiple methods of varying complexity can be employed to combine two or more sets of results of different fidelity into a single data-fit surrogate that can be used for seismic response assessment. For instance, parametric or non-parametric regression analysis (Hastie et al 2009, Weisberg 2005) can be applied in order to combine any number of disparate IM – EDP data into a single functional representation. The functional form of parametric models, e.g. polynomial regression, is predetermined, while in non-parametric ones the predictor does not take a predetermined shape but is constructed based on information derived from the data and can be adjusted to capture any unusual or unexpected features, as in smoothing splines or k-nearest-neighbor regression. The analyst in both cases should avoid including too many parameters in parametric regressions or too much flexibility in non-parametric ones to avoid overfitting, i.e., fitting the random quirks of the dataset while not being able to capture the characteristics of new data points outside the fitted set. When it comes to an error minimization criterion for finding the best-fit function, equal weighting of observations tends to be the typical answer, as in the case of ordinary least squares that minimize the residual sum of squares. Still, this is not necessarily the optimal for our purposes. To better covey the different confidence inherent to results of different fidelity, placing higher weights (e.g. in weighted least squares) on the few high-fidelity results is a more viable option, appropriately biasing the fit towards the points with higher importance.

An alternative non-regression (or non-parametric regression, depending on one's point of view) option is to employ a Bayesian framework (e.g. Jalayer et al. 2011, 2015) to update the probabilistic distribution of a prior estimate of structural response (e.g. obtained by low-fidelity methods) as more (and potentially higher fidelity) data become available. Other methods that do not necessarily include the data-fit surrogate have also been proposed, such as the one of Patsialis and Taflanidis (2020) that utilizes the multi-fidelity Monte Carlo simulation to selectively run analyses on low/high-fidelity models and combine their results for seismic risk assessment. Still, to the authors' belief, the simplest viable solution that can be practically implemented for the problem at hand relies upon fitting the 5-parameter surrogate of Jalayer and Cornell (2009).

The 5-parameter surrogate of Jalayer and Cornell

The 5-parameter surrogate treats non-collapse and collapse data separately: a power-law-based approximation (3 parameters) is fit to the non-collapse data for estimating the distribution of EDP response (and associated probability of exceeding any EDP level) for a certain level of the IM, given that collapse has not occurred. This is augmented by the distribution of collapse-inducing IMs or, equivalently, the probability of collapse given the IM, as determined by fitting an idealized lognormal distribution to the collapse data; effectively two more parameters are added, namely the median value of the distribution and its dispersion. Consequently, a total of 5 parameters fully characterizes the model of demand. The mutually exclusive events of collapse, C, and no collapse, NC, are combined through the total probability theorem to estimate the probability of exceeding any limit state of interest, LS, given the level of the IM:

$$P[EDP > EDP_C \mid IM] = P[EDP > EDP_C \mid NC, IM] \cdot (1 - P[C \mid IM]) + 1 \cdot P[C \mid IM] \qquad (1)$$

where $P[EDP > EDP_C \mid IM]$ is the probability of the demand, EDP, exceeding the EDP capacity, EDP_C, given the IM, and $P[EDP > EDP_C \mid NC,IM]$ is the probability of EDP exceeding EDP_C given the IM and no collapse. The value of 1 stands for $P[EDP > EDP_C \mid C,IM]$ that is the probability of EDP exceeding EDP_C given collapse that always equals 1 and $P[C \mid IM]$ is the probability of collapse given the IM.

The power-law model (Shome and Cornell 1999) is employed for the non-collapse data to estimate the $P[EDP > EDP_C \mid NC,IM]$:

$$EDP = a \cdot IM^{b}\varepsilon \tag{2}$$

where b is the slope in log-log space, ln(a) is the intercept and ε is the regression error, i.e., a lognormal random variable with unit median and a logarithmic standard deviation of $\sigma_{\ln\varepsilon}$. The basic assumption that lies behind Eq. (2) is that the $EDP \mid IM$ dispersion is constant for all IMs, also known as homoscedasticity. However, the dispersion of $EDP \mid IM$ is expected to increase for higher IM values, due to increasing nonlinearilty. In cases of large discrepancies in dispersion at low and high IM values, a separate power-law model can be employed in each region to avoid otherwise complicating its application.

Global collapse is generally deemed to occur when numerical non-convergence appears in a rigorous model that incorporates both material and geometric nonlinearities or when unrealistically large values of EDP appear. To overcome potential bias in the low IMs due to the large near-collapse EDP values, non-collapse and collapse data are treated separately, and the probability of collapse is estimated directly from the collapse points. Multiple methods have been proposed for fitting the collapse data, most notably the logistic regression, the maximum likelihood estimation (MLE) or the method of moments (Baker 2015). MLE can be employed in cases of binary input, such as for the case at hand since records may either cause structural collapse (i.e., 1) or not (i.e., 0), as long as estimates of two numerically different values of collapse probability are available at least at two different levels of IM. The median and the dispersion of the lognormally distributed collapse fragility curve are the parameters that maximize the likelihood function (as per Baker 2015):

$$\left\{\hat{\theta}, \hat{\beta}\right\} = \underset{\theta,\beta}{\arg\max} \sum_{j=1}^{m} \left\{ \ln\binom{n_j}{z_j} + z_j \ln\Phi\left(\frac{\ln\left(x_j/\theta\right)}{\beta}\right) + \left(n_j - z_j\right)\ln\left(1 - \Phi\left(\frac{\ln\left(x_j/\theta\right)}{\beta}\right)\right) \right\} \tag{3}$$

where θ and β are the estimates of the mean, θ, and the standard deviation, β, of the logarithmic collapse fragility distribution, argmax abbreviation stands for maximizing the function, $\Phi(\cdot)$ denotes the cumulative density function of the standard normal distribution, n_j is the number of ground motions per $IM = x_j$, z_j is the number of ground motions that caused structural collapse for $IM = x_j$, and m is the number of IM levels. The probability of collapse can be directly determined via $\hat{\theta}$ and $\hat{\beta}$.

Overall, the 5-parameter surrogate is arguably the minimum comprehensive surrogate that can represent the full-range IM – EDP response space. Adding more parameters, e.g., by augmenting the regression expression of Eq. (2) by more terms, is a natural improvement that may result in a more flexible yet less practical model that would require more data for a reliable fit. Most importantly, employing it with inadequate data may lead to overfitting of the so-called "training" dataset, thus capturing idiosyncratic effects that cannot be generalized. Note here that flexible non-parametric surrogates with an appropriate regularization scheme to avoid overfitting can potentially offer a fully customizable near-automatic regression capability to fit any situation of interest, encompassing both small and large datasets. Still, having only a handful of distinct parameters makes it easier to gain intuition on the effects of our modeling and combination choices and on how to fit each parameter, if needed. Thus, the 5-parameter surrogate is our baseline choice for all subsequent work, offering a good compromise between accuracy and computational effort.

Herein, we propose two ways of how to form mixed surrogate models for seismic response by fitting our baseline surrogate to analysis results from a single case-study building in two distinct situations: (i) combining the results of two different models with different accuracy in disparate regions of response via weighted regression and a user-defined IM-based degree of model preference, and (ii) employing the results of nonlinear static and nonlinear dynamic analysis to directly determine each of the five model parameters.

2 Case-study building

To illustrate the proposed framework, a 4-story RC building is studied. In each principal direction, the building has two perimeter moment-resisting frames (MRFs) of four bays each, as well as internal columns that carry only gravity loads. The plan view of the building and the elevation of the moment frame are shown in **Fig. 1**. The overall plan dimensions are about 55x37m (120'x180') while the total height is about 16.5m (54'), with heights of 4.5m (15') at the first story and 4m (13') for subsequent ones. The building was originally designed by Haselton (2008), while Aschheim et al. (2019) re-designed the structure following a performance-based approach via the use of the Yield Frequency Spectra (Vamvatsikos and Aschheim 2016).

The two-dimensional model of the building is developed in OpenSees software (Mazzoni et al. 2000). Only one out of the two MRFs that act in each principal direction is modeled along with a leaning column. The leaning column is pinned at the foundation and modeled using linear elastic elements having cross sectional properties of one half of the gravity columns of the building plus one half of the columns that belong to the MRFs acting in the other direction. Two 2D distinct models of the case study building are formed (Chatzidaki and Vamvatsikos

2021), one using lumped plasticity elements and another employing distributed plasticity ones, both being viable alternatives for assessment purposes.

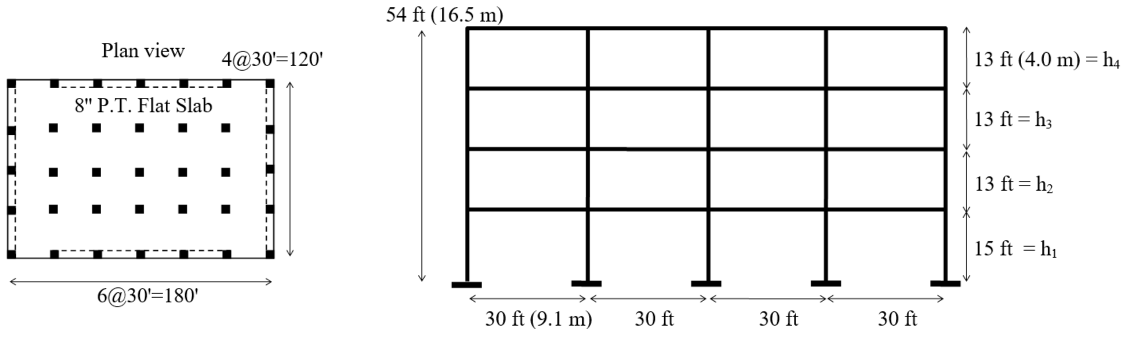

(a) (b)

Fig. 1 (a) Plan view of the building indicating the perimeter frames by dashed lines and (b) elevation of the perimeter moment resisting frame (adopted from Aschheim et al. 2019).

Beams and columns of the distributed plasticity model are modeled using force-based fiber elements discretized into longitudinal steel and concrete fibers. A bilinear constitutive law accounting for pinching and stiffness degradation is employed to model the steel reinforcing bars. The cover concrete is modeled without confinement, while the confinement-related parameters of the core concrete are calculated per Mander et al. (1988). The strength of the steel and concrete materials is set at their expected values, rather than nominal characteristic strengths, thus f_{ye} = 475MPa (69ksi) and f_{ce} = 44.8MPa (6.5ksi). The rigid diaphragm is simulated via stiff truss elements connecting the frame nodes at each floor level. One end of each horizontal beam element is provided with a low stiffness axial spring at the connection with the column. This solution is preferred instead of imposing rigid kinematic constraints, since they would impose the condition of zero axial strain on beams resulting in the generation of fictitious axial compression forces that would artificially increase the bending moment capacity of beam sections. Rayleigh damping of 1% is assigned to the first and second mode. Although this is lower than a typical value of 5% usually assigned to RC structures, it is considered realistic as cracking is directly incorporated in the fiber model giving rise to early hysteretic damping (Sousa et al. 2020).

Beams and columns of the lumped plasticity model are realized by a single force-based beam-column element per member with plastic hinges located at each end. Moment-rotation laws for each plastic hinge are defined in terms of the backbone curve of ASCE 41-13 (2014). Rigid kinematic constrains are applied on all nodes of each floor thus enforcing the same lateral displacements. A minor calibration of the elastic member stiffness is employed to avoid a large mismatch in the periods of the distributed and lumped plasticity models. Specifically, the "cracked" moment of inertia of both lumped plasticity beams and columns is determined by averaging the initial "uncracked" stiffness and the nominal "cracked" stiffness at yield, as derived by moment-rotation analyses of the actual fiber sections. A Rayleigh damping of 5% is assigned in the first and second mode for the lumped plasticity model. In all cases, P-Δ effects are accounted for via a first-order treatment.

The SPO capacity curves resulting from a first-mode-proportional lateral load pattern are shown in **Fig. 2** for both models, in terms of base shear, V_{base}, and roof drift ratio, θ_{roof}. The fundamental periods of the distributed and the lumped plasticity models are $T_{1,f}$ = 0.79sec and $T_{1,l}$ = 0.97sec, respectively. Incremental Dynamic Analysis (IDA, Vamvatsikos and Cornell 2002) is performed on both models to compare their respective response. The far-field ground motion set of FEMA P695 (FEMA 2009) is used for the analysis; it comprises 22 ground motions, each having two horizontal components, resulting in a total of 44 accelerograms. To facilitate comparison between the two models, a common IM is adopted that is the average spectral acceleration (*AvgSa*, see Kohrangi et al. 2017) for the period range [0.3sec, 3.0sec] with an increment of 0.1sec. For illustration purposes, the individual IDA curves for the maximum interstory drift ratio, θ_{max}, along with the 16, 50 and 84% fractiles are presented in **Fig. 3**a-b for the lumped and the distributed plasticity models, respectively.

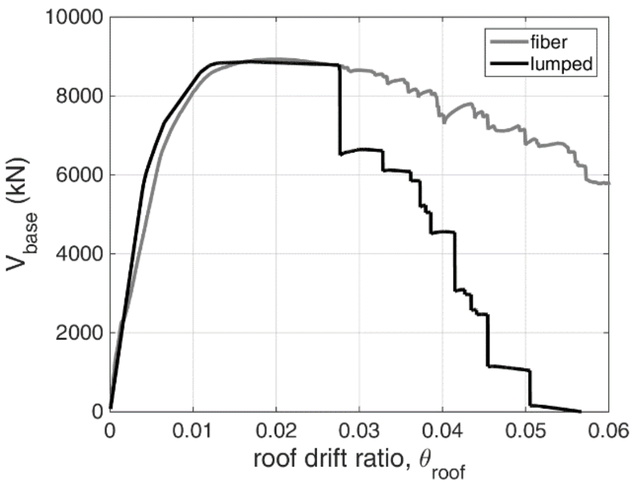

Fig. 2 Static pushover capacity curves of the distributed plasticity model (grey line) versus the lumped plasticity model (black line).

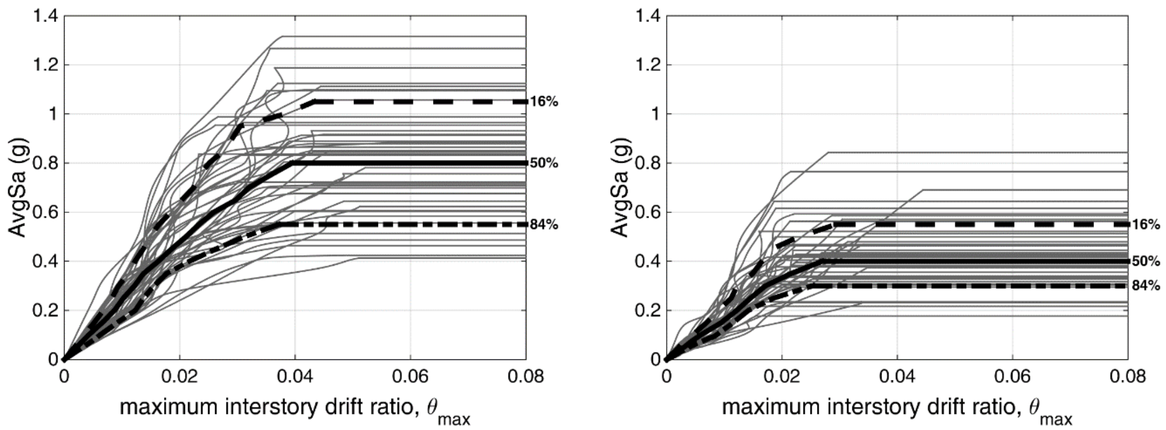

(a) lumped plasticity model (b) distributed plasticity model

Fig. 3 IDA results of the (a) lumped plasticity model and (b) the distributed plasticity model in terms of *AvgSa* and θ_{max} along with the 16%, 50% and 84% IDA fractiles.

3 Application 1: Mixing structural models of different accuracy

The lumped and the distributed plasticity models offer different accuracy and convergence capabilities in the complementary response regions of low versus high IMs (and EDPs). Specifically, the distributed plasticity models allow representation of phenomena such as concrete cracking and gradual plastification of sections, thus they can better reproduce the behavior of the structure in the pre-yield segment. However, they cannot capture the post-capping response of the system and they often fail to converge in the region of negative global lateral stiffness. On the contrary, phenomenological lumped plasticity elements can model the post-capping response but often fail to capture the transition of the system from the initial uncracked stiffness to the cracked one, thus they cannot fully reproduce the pre-yield structural behavior (Haselton et al. 2007). At the same time, they offer easier convergence, thus they can be applied when NRHA is performed to assess the structural behavior even close to collapse.

Given the relative strengths and weaknesses of each modelling type, we expect different degrees of bias in the estimation of EDP response given the IM level. For low IMs, the lumped plasticity model cannot capture the pre-yield evolution of member stiffness, thus leading to lower, or unconservatively biased, variability estimates. This tendency is evident in the IDA curves, especially when plotted in terms of 5%-damped first-mode spectral acceleration $Sa(T_1, 5\%)$. It can only be partially observed in **Fig. 3**a-b due to the use of *AvgSa* as the IM, which tends to increase the record-to-record variability in the elastic range, involving, e.g., “elongated” periods that only become relevant after yield. A higher median EDP response is also observed for the distributed plasticity model. Although this latter observation is not necessarily generalizable, it surely tells us that, for the case at hand, the lumped plasticity model underestimates both the median and the dispersion of EDP given IM. For higher IMs, the distributed plasticity model is clearly disadvantaged by its propensity for non-convergence, being unable to reliably predict the post-capping response. It offers conservative biased-high estimates of EDP given IM, or conversely biased-low estimates of the distribution of IM given EDP for practically any fragility in the post-capping region.

The aforementioned observations can cast doubt on the suitability of either single model for fragility assessment, and point to the potential for improvement by combining their respective results. As a minimalistic example, in the spirit of multi-stripe analysis (MSA, Jalayer and Cornell 2009), we shall employ two stripes of EDP given IM from each model, as schematically presented in the conceptual algorithmic process of **Fig. 4**. The lower stripes come from the distributed plasticity model and target the pre/near-yield response, while the two higher stripes come from the lumped plasticity model to better capture the post-yield and near-collapse behavior. More stripes, cloud analysis (Jalayer 2003) or IDA can also be employed, to obtain the IM – EDP representation of the source models. Even different methods can be adopted for the two source models without problems. In the end, we seek to determine a single 5-parameter surrogate that incorporates both sets of results to optimally determine the fragilities of interest.

Weighted regression is our method of choice for fitting the 5-parameter surrogate to combine the outputs of the lumped and the distributed plasticity models. This is fairly straightforward for fitting collapse-level data, as one would expect to derive the collapse fragility based on the more reliable model for that range of response, thus giving full weight to the lumped plasticity model. Assigning model weights *a priori* to non-collapse results is a more difficult premise. For instance, if N low-fidelity data points are to be mixed with $M << N$ high-fidelity points, the higher number of low-fidelity points will dominate the result, unless a significantly higher weight is assigned to the few high-fidelity points, so that they can still have an impact on the mixed model. Similarly, when EDP results at multiple IM levels are mixed, a few high IM and EDP values can have a disproportionally higher leverage relative to the lower ones, easily acting as outliers that can dominate the regression, potentially causing bias in low-IM estimates of response. Finally, the fragilities targeted also play a role; for example, one would emphasize the lower IM stripes if mainly serviceability level limit-states are of interest.

As a potential solution, we propose the concept of an IM-based Degree of Preference (DOP), whereby a user declares his/her relative confidence per model given the IM level. Then, a direct search optimization algorithm is employed for determining near-optimal regression weights that minimize the difference among the mixed model's fragility and the target/ideal fragilities as computed based on the DOPs.

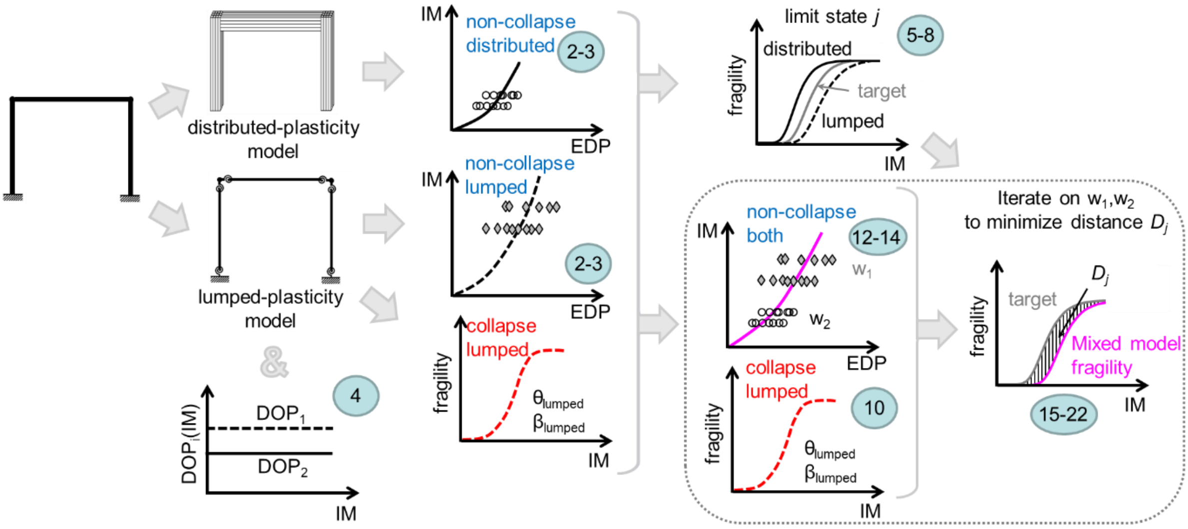

Fig. 4 Conceptual approach for mixing structural models of different accuracy via the 5-parameter model. The numbers indicate the corresponding steps of the WeightSearch algorithm.

Degree of preference, target fragilities, and optimal mixing weights

The DOP is loosely defined as the analyst's degree of belief on the applicability of each source model given the IM level. Mathematically speaking, it is a function, $DOP_i(IM)$, per each model $i = 1,\ldots, N$, where:

$$0 \le DOP_i(IM) \le 1, \qquad \sum_{i=1}^{N} DOP_i(IM) = 1 \tag{4}$$

It may have any shape, but complicated functions are not recommended unless they have an explicit physical meaning. For our purposes, a linear function will be adequate.

A definition akin to Eq. (4) but parameterized on the EDP may seem to be more straightforward, as specific EDP thresholds can better (and *a priori*) delineate regions of differing structural behavior compared to IM thresholds. However, this can become problematic if MSA is applied with records coming from a hazard-consistent selection process (e.g., Lin et al 2013a,b). Then, placing differing weights on the results of records selected as a single set may cause inconsistency with the hazard, partially defeating the purpose of selection. To avoid such pitfalls and any associated complex workarounds, we shall opt for the practicality of $DOP_i(IM)$ rather than the intuitive simplicity of $DOP_i(EDP)$.

The purpose of the DOP is to allow estimating an intermediate proxy, termed the target fragility curve, $P_{tgt,j}[EDP > EDP_{C,j} \mid IM]$, for limit state j characterized by a threshold EDP capacity of $EDP_{C,j}$, by combining the corresponding fragilities $P_{i,j}[EDP > EDP_{C,j} \mid IM]$ of the source models weighted by the DOP of each model as:

$$P_{tgt,j}[EDP > EDP_{C,j} \mid IM] = \sum_{i=1}^{N} DOP_i\left(IM\right) \cdot P_{i,j}[EDP > EDP_{C,j} \mid IM] \tag{5}$$

Fig. 5 shows two examples of DOP functions as well as the corresponding target fragility curves that are computed via Eq. (5). Specifically, **Fig. 5**b shows the target fragility curve when constant DOPs are assumed (**Fig. 5**a), while **Fig. 5**d shows the target fragility when linear DOP functions are adopted that range from 0 to 1 (**Fig. 5**c).

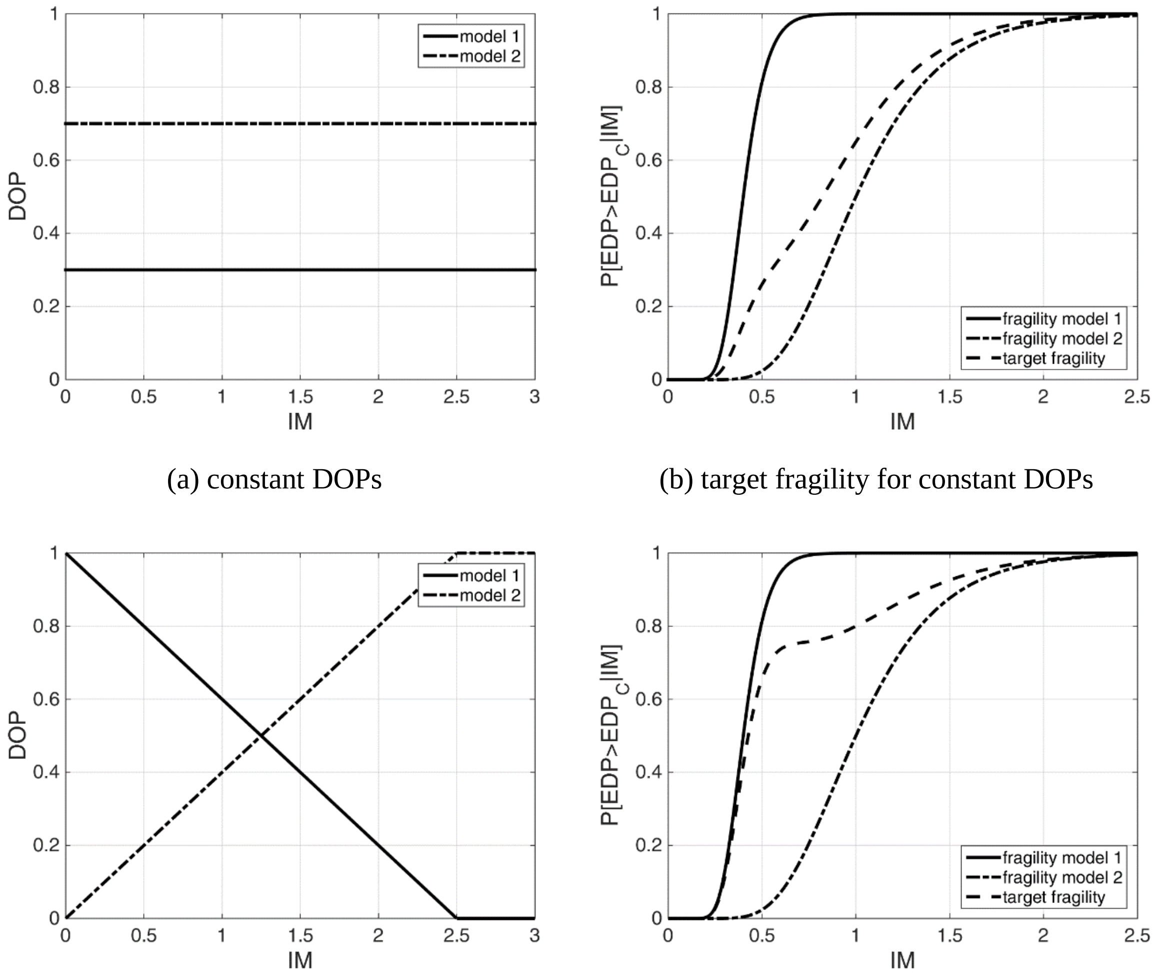

(a) constant DOPs

(b) target fragility for constant DOPs

(c) ramp DOPs

(d) target fragility for ramp DOPs

Fig. 5 Two examples of DOPs and the resulting target fragilities for combining two arbitrary models, 1 and 2. The constant DOPs of (a)-(b) imply a consistent preference of model 2 over model 1 for any IM. The ramp DOPs of (c)-(d) assume that the fidelity of model 2 increases over model 1 with the IM level.

The target fragility is not necessarily what one would like to employ as the final fragility estimate, as for some DOP choices it may not even resemble a traditional fragility; it is only a proxy to help us determine the candidate fragility that best matches the analyst's preference. For any given limit-state this is achieved by selecting the mixed-model fragility $P_{mixed,j}[EDP > EDP_{C,j} \mid IM]$ having the minimum "distance" D_j from the target fragility. Several options are available to quantify the difference of the two distributions. Potential choices are the relative entropy or Kullback-Leibler divergence (Tsioulou and Galasso 2018), the Cramer-Von Mises distance (Parr 1981), and the absolute area difference. The latter, is simply the integral of the absolute difference between the two cumulative distribution functions, and it is our baseline choice:

$$D_j = \int_0^{+\infty} \left| P_{tgt,j}\left[EDP > EDP_{C,j} \mid IM\right] - P_{mixed,j}\left[EDP > EDP_{C,j} \mid IM\right] \right| \mathrm{d}IM \tag{6}$$

One may further refine the distance metric of Eq. (6) by emphasizing divergence in the lower left tail, which often figures more prominently in risk assessment (due to the higher frequency of the IM level) than the corresponding right tail.

Minimizing Eq. (6) separately per each limit-state fragility $j = 1,\ldots,M$ would lead to M different 5-parameter surrogates and corresponding weights for their fitting. Instead, for reasons of logistical simplicity, a single mixed model (and set of weights) may be employed to determine all limit-state fragilities. Then one should seek to minimize a combination of all D_j, such as D_{tot}, the sum of the distances for all limit states of interest:

$$D_{tot} = \sum_{j=1}^{M} D_j \tag{7}$$

Having all our machinery in place, it now becomes a straightforward application of direct search to determine optimal (or near-optimal) weights for the model mixing, as indicatively presented for mixing two source models via the WeightSearch algorithm, following the conceptual model of **Fig. 4**:

Algorithm WeightSearch: Selection of near-optimal mixing weights for two source models

1 **for** i = 1 to 2 source models
2 obtain the IM-EDP pairs of source model i
3 fit the 5-parameter surrogate to source model i
4 determine the $DOP_i\,(IM)$
5 **for** j = 1 to M limit states
6 calculate i-th source fragilities $P_{i,j}[EDP > EDP_{C,j}\,|\,IM]$ from the 5-parameter surrogate
7 calculate $P_{tgt,j}[EDP > EDP_{C,j}\,|\,IM]$ via Eq. (5)
8 **end for**
9 **end for**
10 select the mixed model's collapse fragility $P[C\,|\,IM]$ from the most reliable source model for collapse
11 **for** k = 1 to K weights
12 assign weight $w_1 = 1/(2K) + (k\text{-}1)/K$ on the non-collapse data of source model 1
13 assign weight $w_2 = 1 - w_1$ on the non-collapse data of source model 2
14 fit the 3-parameters of Eq. (2) via (w_1, w_2)-weighted regression
15 **for** j = 1 to M limit states
16 calculate mixed fragility $P_{mixed,k,j}[EDP > EDP_{C,j}\,|\,NC, IM]$ from the fitted 3-parameters
17 find $P_{mixed,k,j}[EDP > EDP_{C,j}\,|\,IM]$ via $P_{mixed,k,j}[EDP > EDP_{C,j}\,|\,NC, IM]$ and $P[C\,|\,IM]$ via Eq. (1)
18 calculate $D_{j,k}$ via Eq. (6)
19 **end for**
20 calculate $D_{tot,k}$ via Eq. (7)
21 **end for**
22 select weight combination k corresponding to the minimum $D_{tot,k}$

As the very first step of the WeightSearch algorithm we need to determine IM – EDP pairs for each source model. To do so effectively, we need to keep in mind the end game of step 3, i.e., fitting a 5-parameter surrogate per source. Given the differing predictive power of the source models, it actually makes sense to fit only the non-collapse part of Eq. (2) for the distributed plasticity model, i.e., only 3 parameters, effectively assuming that the probability of collapse is zero, and both parts (all five parameters) for the lumped plasticity. Of course, this means that the source fragilities determined in step 6 for the distributed plasticity model make little sense for large EDP_C values near collapse. Yet, this is of little concern if an appropriate DOP is selected that deemphasizes the distributed plasticity model results for high IM values, e.g., as in **Fig. 5**c, thus allowing the target fragility of step 7 to be dominated by the lumped plasticity model at high IMs. Following the pre-processing part of steps 1-9, we select the collapse fragility of the lumped plasticity model for the mixed model in step 10, and then we enter the direct search of steps 11-21, iteratively trying K different weight combinations, and culminating in step 22 with the selection of those that provide the lowest total distance, D_{tot}, from the target fragilities.

Note that a prerequisite of applying the WeightSearch algorithm is being able to fit at least the non-collapse part of the 5-parameter surrogate to both source models, thus being able to actually derive fragilities from both. Where insufficient data is available to allow such fitting per source, as in the case of having just a few sparse time history analyses, only one or two parameters out of the three in Eq. (2) may be fitted. Then, the DOP approach is an overkill, and *a priori* weight assignments may be preferable or even more intuitive, as will be discussed in the second application example (Section 4).

Application to the case-study building

The IM – EDP characterization for the case study building is determined by performing two stripes of analyses on each source model. An interesting question of computational significance is how many records to use per stripe. An optimal number would depend on parameters such as the type of the structure, as well as the IM and EDP used. In our case we have selected relatively well-behaved variables for the IM and EDP, i.e., *AvgSa* and $\theta_{\max}$, with dispersions in the order of 30-40%. In similar EDP situations, Baltzopoulos et al. (2018) employed a minimum of 20 records per stripe. In our case, thanks to the good performance of *AvgSa* and to showcase a relatively frugal application, a single set of 9 ground motion records is adopted that are randomly selected out of the 44 records of FEMA P695. Taking in regard the relative advantages of each model, the stripes of the distributed plasticity model are performed at relatively low *AvgSa* values equal to 0.10g and 0.15g, while higher values of 0.60g and 1.00g are employed for the lumped plasticity model, aiming to capture the behavior closer to the collapse region, as shown in **Fig. 6**.

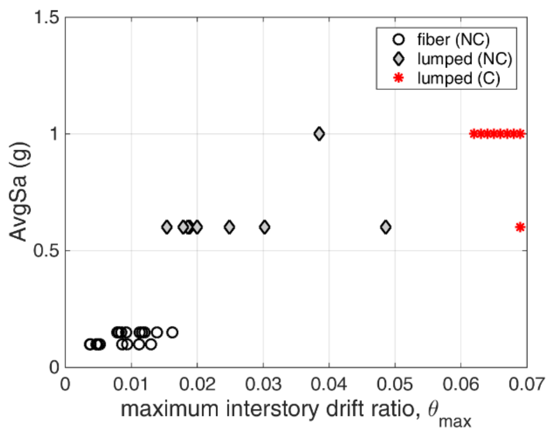

Fig. 6 The four IM-EDP stripes, showing both collapse (C) and non-collapse (NC) points.

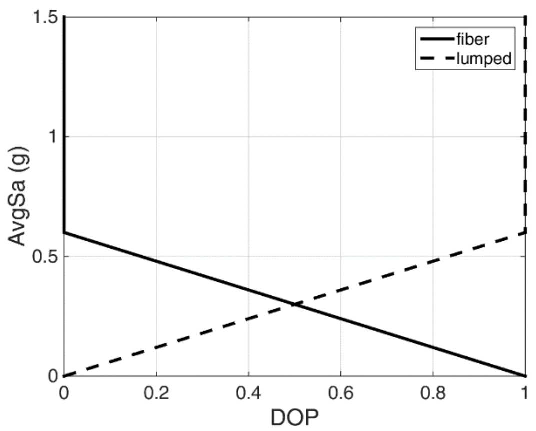

Fig. 7 DOPs assumed for the distributed and the lumped plasticity model.

The power-law fit of the non-collapse data is presented in **Fig. 8** for the lumped and the distributed plasticity models. Only the first stripe, i.e. at 0.6g, is considered in the non-collapse fit of the lumped plasticity model assuming $b = 1$, while the other one having more than 16% of collapses is omitted. In the low-IM stripes of the distributed plasticity model, all records achieved convergence; thus unreliable "collapse" points did not appear. If that was not the case, such data would be neglected in the fitting of the collapse fragility, effectively assigning a weight of 1.0 to the lumped plasticity estimates of collapse. In the high-IM stripes of the lumped plasticity model, both collapse and non-collapse points appeared. Furthermore, each stripe has a different percentage of collapsed points. Had the same percentage been estimated, we would either have to add more records to the two stripes, or simply add a new stripe to be able to achieve a full-range estimate of the collapse fragility.

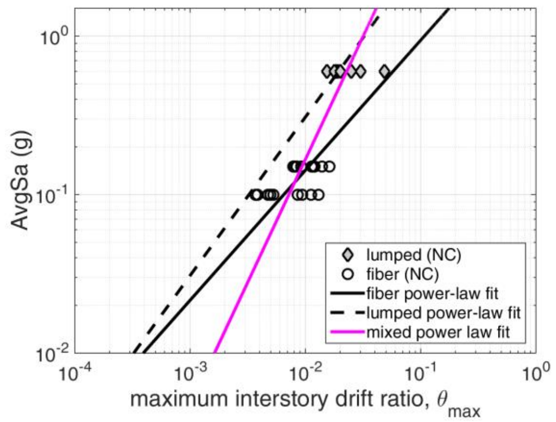

Fig. 8 Non-collapse IM – EDP pairs from the lower three stripes of **Fig. 6**, as considered in the power-law fit of the lumped plasticity (dashed line) and the distributed plasticity model (continuous line). The power-law based approximation of the mixed model is also presented in magenta.

Having established the IM – EDP points, the relative DOPs are assumed to follow a ramp pattern, linearly varying within 0g and 0.6g and remaining constant thereafter as shown in **Fig. 7**. This corner IM point is selected to be at the level of the first high-IM stripe employed for the lumped plasticity model. Different choices would obviously present different final results, still there is a wide range of IMs where the precise corner point value is of secondary importance.

Herein, a single mixed model is to be determined for the four limit states considered at θ_{max} capacities, $\theta_{max,C}$ = 0.015, 0.02, 0.025 and 0.030. The source fragilities, resulting from fitting the power-law approximation on the distributed plasticity model and the 5–parameter surrogate to the lumped plasticity model, are presented in **Fig. 9**a-d for all limit states of interest. The target fragilities resulting from combining the fragilities of the source models based on the pre-defined DOPs via Eq. (5) are then determined. Their shape does not necessarily resemble the "classic" S-shaped fragilities (**Fig. 9**a), or even conform to the monotonicity expected of a fragility curve (**Fig. 9**b-d), due to the DOPs ramp-shape. Still, this is of no concern, as the target fragility is only meant to serve as a simple proxy.

The mixed model non-collapse fit that offered the fragilities best matching the target curves (i.e., with the lowest total distance D_{tot}) is presented in **Fig. 8**. The resulting mixed fragility curves lie between the source fragilities in all cases, as shown in **Fig. 9**a-d. As required, they all lean towards the distributed plasticity model for lower IMs, and veer off towards the more reliable lumped plasticity model at higher IMs, with this change occurring earlier (in IM terms) as a higher-damage fragility is sought. To achieve this transition within the constraints of the 5-parameter model, the mixed curves show a larger dispersion compared to the source ones, necessitated by the need for a shallower slope around the median to capture the two different source models. As a result, at the low left tail, some minor overlapping of the mixed fragilities and the distributed plasticity source fragility occurs. If this is undesirable, given the significance of the lower tail for risk assessment, additional constraints may be added to the optimization algorithm.

The median and dispersion values, assuming lognormality, of the fragility curves for the lumped, the fiber and the mixed model for all limit states are listed in **Table 1**. The fiber model shows constant dispersion per the non-collapse power-law model while this constant dispersion is further modulated by the collapse fragility in the case of the lumped-plasticity model. Note how in the latter case the dispersion decreases with the IM as *AvgSa* is better performing away from the elastic region where "elongated periods" captured by *AvgSa* come into play. The mixed model, by virtue of combining both models, naturally employs a larger starting dispersion that converges to the lower lumped-plasticity dispersion close to collapse.

Countless other improvements can be incorporated, ranging from using different surrogates as a basis, to mixing more models and using different weighting approaches. These will probably come out naturally as different applications are tackled. Still, even the baseline approach proposed herein is enough to generate a single mixed model surrogate from disparate sources that conforms to the model with the higher validity in each region of response.

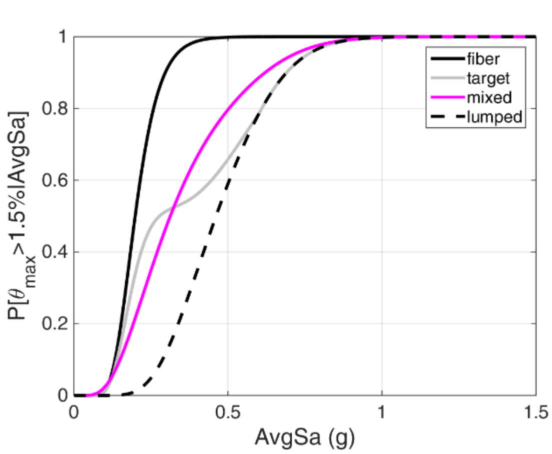

(a) fragility curves for $\theta_{\max,C}$ = 1.5%

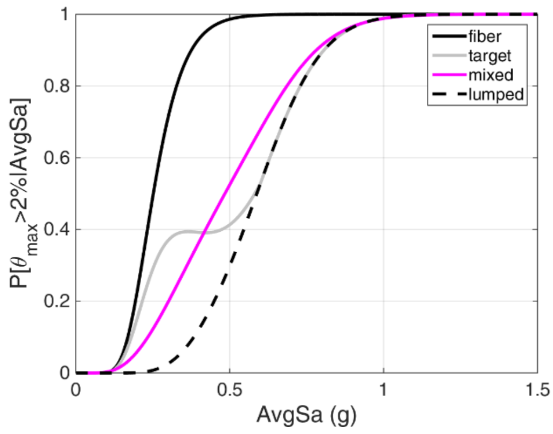

(b) fragility curves for $\theta_{\max,C}$ = 2.0%

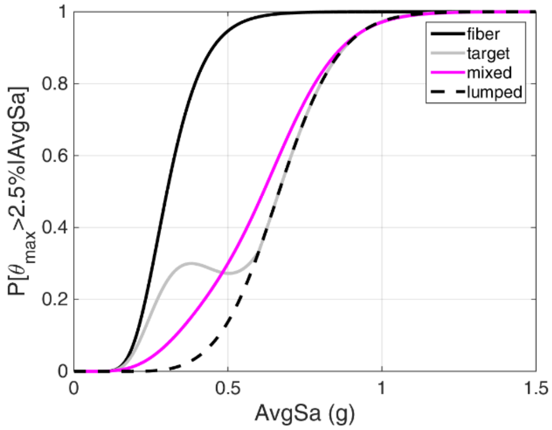

(c) fragility curves for $\theta_{\max,C}$ = 2.5%

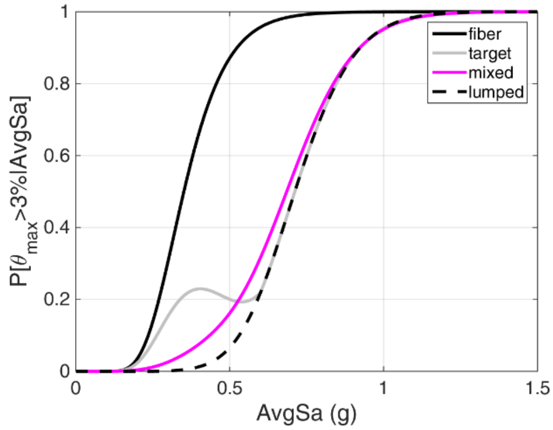

(d) fragility curves for $\theta_{\max,C}$ = 3.0%

Fig. 9 Fragility curves for all examined limit states. For each limit state the two source fragilities, the target, and the mixed fragility are presented.

Table 1 Fragility curve median and dispersion values in terms of *AvgS*a, assuming lognormality, for all models and limit states.

Model / Limit State	Fiber	Lumped	Mixed
$\theta_{\max,C}$ = 1.5%	0.20 (31%)	0.46 (34%)	0.31 (56%)
$\theta_{\max,C}$ = 2.0%	0.25 (31%)	0.59 (29%)	0.48 (48%)
$\theta_{\max,C}$ = 2.5%	0.30 (31%)	0.67 (24%)	0.62 (37%)
$\theta_{\max,C}$ = 3.0%	0.35 (31%)	0.71 (21%)	0.69 (28%)

4 Application 2: Mixing different structural analysis types

The approximation of the multi degree-of-freedom (MDOF) structure via an equivalent single degree-of-freedom (ESDOF) model renders SPO analysis the preferred option for many applications since it offers computational simplicity and can be implemented with ease. In the context of seismic codes (e.g., ASCE 41-13, 2014 or EN1998-3, 2005), SPO is used to provide a single estimate of the EDP response for a given level of seismic intensity, yet it is often disregarded that the ESDOF approximation can also be adopted to comprehensively assess the dynamic response of the structure. This SPO/ESDOF approach requires following a procedure similar to the one appearing in current codes, namely (i) performing SPO analysis on the MDOF structure, (ii) obtaining the SPO curve of the ESDOF system, (iii) fitting a piecewise linear function to the SPO curve, (iv) estimating the seismic demand of the ESDOF system based on the SPO curve, and (v) translating the ESDOF seismic demand to the MDOF response.

The important difference between typical code-style application and a full-range estimation comes in the fourth step, i.e., the estimation of ESDOF seismic demand. Typically, one would employ R-μ-T (strength ratio-ductility-period) relationships to determine a central value (mean or median) of the ESDOF displacement response given the intensity level of interest, usually in terms of $Sa(T_1, 5\%)$ (see Miranda 2001 and references therein). Instead, the full distribution of demand can also be obtained. This is typically assumed to follow the lognormal distribution, characterizing the $EDP \mid IM$ response by two parameters, i.e., the conditional mean and variance. Both parameters can be assessed either by subjecting the ESDOF to a number of dynamic analyses, e.g., via the open-source tools developed by Baltzopoulos et al. (2018), Elkady and Lignos (2018), or by employing advanced R-μ-T relationships, such as the ones proposed by Ruiz-García and Miranda (2007) for elastoplastic oscillators, or the SPO2IDA tool (Vamvatsikos and Cornell 2006, Baltzopoulos et al. 2016) for oscillators with complex quadrilinear backbones.

Assessing the MDOF response using the ESDOF as a basis inevitably brings in all the weaknesses associated with the ESDOF approximation of the mean and/or variance of dynamic response. The ESDOF model cannot accurately reproduce complex dynamic characteristics of the MDOF, potentially resulting in biased mean estimates of the seismic demand, especially in cases of tall or plan-asymmetric buildings. Regarding variance, the ESDOF model can only capture the record-to-record variability in the first-mode, while being unable to reproduce the additional variability contributed by higher modes.

These issues reduce the fidelity of SPO-based results and render one unable to recommend the SPO/ESDOF approach with some confidence as a generally viable method. The question, thus, remains: Can one still ride this trusty old workhorse of seismic assessment to deliver credible results in a performance-based world? Perhaps yes, with a pair of new horseshoes. In this regard, Baltzopoulos et al. (2017) proposed a methodology to assess the missing variability in the elastic range and inject it back into the SPO/ESDOF estimate, using precomputed dynamic analysis results of simplified MDOF systems. Similarly, a limited number of “just-in-time” computed dynamic analyses of the MDOF model can be employed to refine the SPO/ESDOF mean estimate of response. This allows taking advantage of the full-range computational capability of the ESDOF and then bias-correcting the less-than-ideal estimate using MDOF results. In line with our mixed model concept, a minimalistic approach is offered herein to combine pushover and dynamic analysis source results into a single mixed 5-parameter surrogate that is suitable for fragility assessment, as schematically presented in the flowchart of **Fig. 10**. This approach is illustrated by means of an example for the lumped plasticity model of the case-study building.

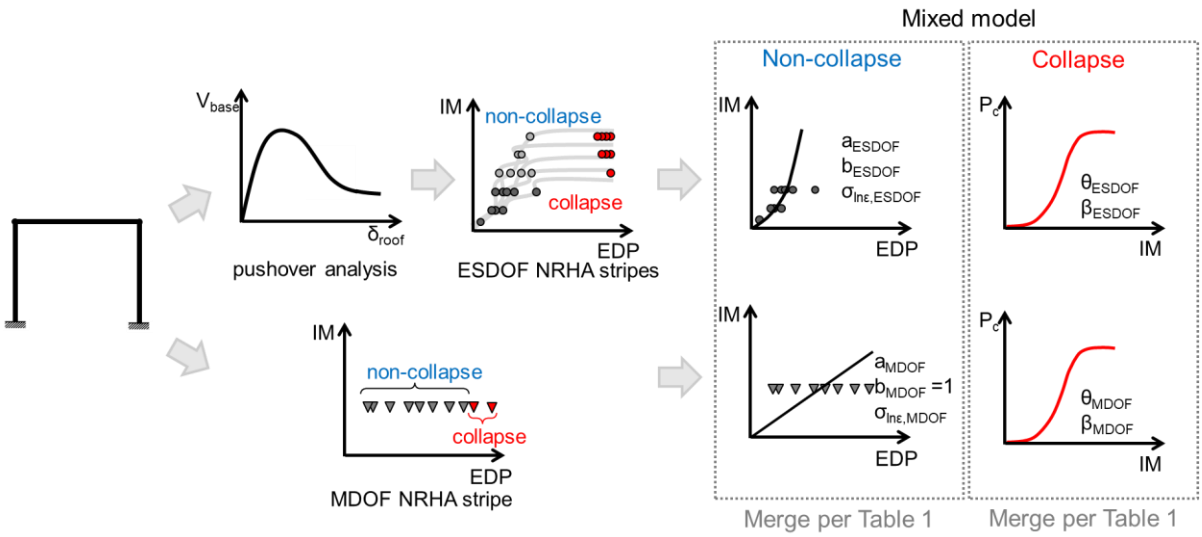

Fig. 10 Conceptual flowchart of mixing structural analyses of different accuracy: the case of static pushover and nonlinear response history analyses.

The SPO-based approximation of IDA

The SPO analysis of the MDOF model (**Fig. 11**a) is used as a basis to determine the backbone curve of the ESDOF oscillator, e.g., following the recommendations of Fajfar (2000): The MDOF V_{base} and roof displacement are divided by the first-mode participation factor, Γ, while the first-mode effective mass, m^*, is adopted for the oscillator. To achieve a simpler representation of the ESDOF backbone, a piecewise linear function can be fitted. For the case at hand, a bilinear backbone curve is adopted. De Luca et al. (2013) suggested that the elastic segment of bilinear backbones should match the elastic stiffness of the SPO curve, especially for structures that are not characterized by significant stiffness changes. This is the expected behavior of the case-study lumped plasticity model since by its nature it cannot reproduce concrete cracking and gradual plastification of sections, thus resulting in minor stiffness changes in the elastic range. Consequently, the elastic segment of the bilinear fit is selected to match the initial stiffness of the SPO curve. The post-yield linear segment of zero stiffness matches the maximum base shear and the horizontal plateau ends at the deformation limit of 0.33 where more than 20% of the maximum base shear is lost per De Luca et al. (2013). The resulting SPO of the ESDOF model as well as its bilinear fit are presented in **Fig. 11**b. Given the nominal yield displacement, δ_y^*, and yield force, F_y^*, the resulting period, T^*, of the ESDOF is estimated as $T^* = 2\pi\sqrt{m^*\delta_y^*/F_y^*}$, almost perfectly matching the MDOF's T_1 by construction; thus, they are going to be used interchangeably henceforth.

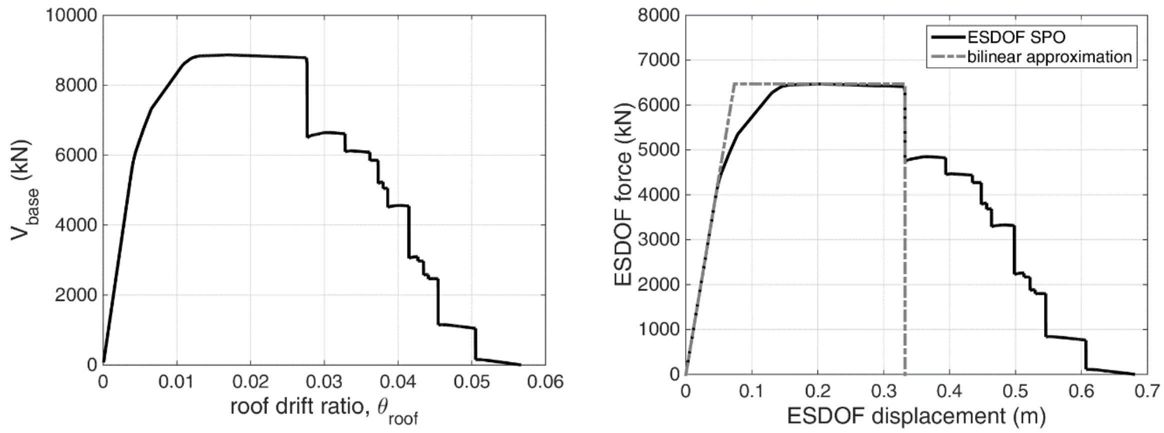

(a) MDOF (b) ESDOF

Fig. 11 Static pushover curve of (a) the lumped plasticity model and (b) its bilinear fit in ESDOF terms.

For illustrative purposes, and to dispense with any further approximations introduced even by elaborate R-μ-T relationships such as SPO2IDA, the bilinear-backbone ESDOF is directly subjected to IDA to assess its seismic response using the far-field ground motion set of FEMA P695. The resulting IDA curves are presented in **Fig. 12**a along with their 16%, 50% and 84% IDA fractiles in terms of $Sa(T_1, 5\%)$ and $\theta_{\max}$, where T_1 is the period of the lumped plasticity MDOF model. A cut-off limit is employed in IDA results for ESDOF displacement equal to 0.33, as imposed by the ultimate ductility of the fitted bilinear backbone (**Fig. 11**b). The grey rectangle of **Fig. 12**a highlights that all IDA fractiles of the SPO/ESDOF approach coincide for low $Sa(T_1, 5\%)$ values, where the ESDOF behaves elastically thus resulting in zero response variability.

For comparison purposes, IDA curves and IDA fractiles are also presented in **Fig. 12**b for the lumped plasticity model in terms of $Sa(T_1, 5\%)$ and θ_{max}. The 50% IDA fractile of the SPO/ESDOF approach appears somewhat shifted to the left in respect to that of the MDOF, indicating that bias is introduced in the median SPO/ESDOF estimate. In any case, obtaining the same median estimate from the two different approaches would be quite fortuitous since multiple approximations are involved in the SPO/ESDOF. Herein this results in underestimation of the true MDOF response. While this outcome tends to occur fairly often, it cannot be generalized as it is attributed to many user-selected factors. One is the fitting of the oscillator backbone, with different fits resulting to changes in the SPO/ESDOF estimates. Another could be the lateral load pattern used in the SPO analysis. In our case, a first-mode proportional lateral load pattern is adopted, but adaptive load patterns that allow accounting for stiffness changes, changes of the modal characteristics and period elongation of the structure (Elnashai 2001) could potentially better reproduce the behavior of the MDOF in the negative stiffness segment. Regardless of the approach adopted, such bias should always be expected when an ESDOF is used in place of the MDOF; it is of more interest now to show how one can take advantage of the higher-fidelity MDOF model to bias-correct the SPO/ESDOF estimate at a low computational cost.

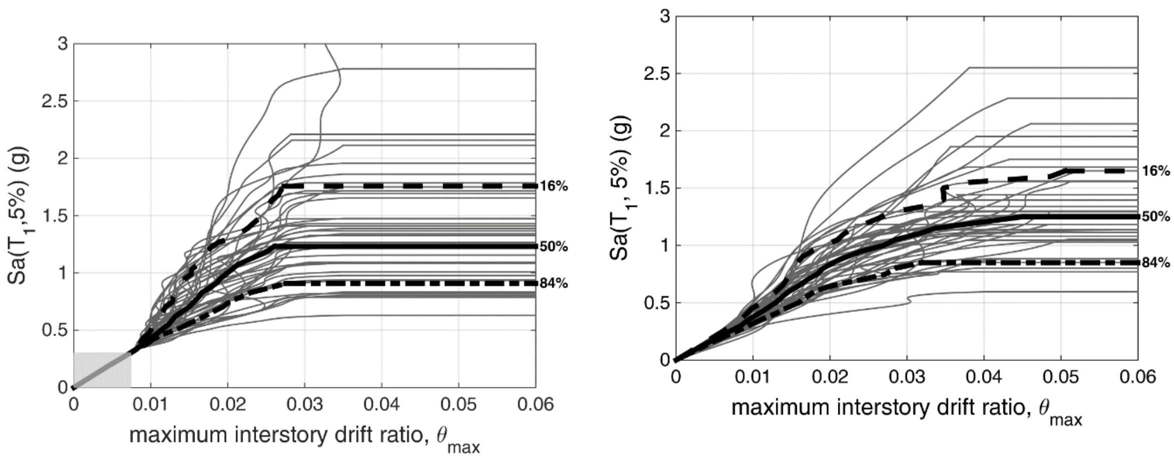

(a) SPO/ESDOF (b) MDOF

Fig. 12 IDA analysis results (grey) and 16%, 50% and 84% IDA fractiles (black) from (a) the SPO/ESDOF approach (with a grey rectangle showing the area of pure linear-elastic response) versus (b) the MDOF model.

Bias-correction via a single MDOF stripe

Any number of MDOF analyses can be employed to improve upon the SPO/ESDOF results. Ideally, one could employ several MDOF stripes or even a cloud of MDOF data and combine them within a weighted regression scheme (similar to Section 3) to determine the mixed model per a user's preferences. Still, as the number of MDOF analyses increases, the usefulness of the SPO/ESDOF combination disproportionately diminishes. Frugal options are of more practical interest.

Actually, even a single stripe of, say, five to ten MDOF dynamic analyses can offer usable information on the seismic response. Assuming mostly non-collapse points are recorded, such a limited number of analyses can typically provide a better estimate of the median $EDP\,|\,IM$ response than the SPO/ESDOF, but not necessarily of the dispersion, which tends to be underestimated by small samples. Still, there are cases where even small samples can provide a viable estimate of the dispersion, for instance, if ground motion records are selected via a stratified (rather than random) sampling scheme, as performed, e.g., by the Conditional Spectrum approach (Lin et al. 2013a,2013b, Kohrangi et al. 2017). Then, a stripe of ten MDOF analyses may offer a competitive estimate of dispersion. Nevertheless, for reasons of generality the MDOF model is only employed herein for updating the median non-collapse response estimate and/or the collapse fragility. Therefore, the MDOF stripe results are *selectively* assimilated into the 5-parameter surrogate as shown in **Table 2**.

Table 2 Source model used to compute each parameter of the mixed 5-parameter surrogate.

Data (Fit)	Parameter	MDOF or SPO/ESDOF model?
Non-collapse data (power-law regression fit)	a	if $P_{stripe} \leq 0.16$ then MDOF, else SPO/ESDOF
	b	SPO/ESDOF
	$\sigma_{\ln\varepsilon}$	SPO/ESDOF
Collapse data (lognormal MLE fit)	θ	if P_{stripe} in [0.2, 0.8] then MDOF, else SPO/ESDOF
	β	if P_{stripe} in (0,0.2) or (0.8,1) then MDOF, else SPO/ESDOF†

† if $P_{stripe} = 1$ the MDOF stripe is mostly discarded

The probability of collapse of the MDOF model, $P_{\text{stripe}} = P[C\,|\,IM{=}IM_{stripe}]$, given the stripe's IM level, IM_{stripe}, can be directly computed as the fraction of ground motion records that cause structural collapse out of the total number of records used in the stripe. Depending on the value of P_{stripe}, the MDOF model can be used to update the non-collapse and/or collapse estimate obtained by the SPO/ESDOF, as presented in **Table 2**. In general, if a single stripe is to be performed on the MDOF model, the IM_{stripe} should be selected so that the resulting P_{stripe} is preferably lower than 0.5, and optimally lower than 0.16, since in the latter case the

MDOF can also be used to bias-correct the non-collapse estimate obtained by the SPO/ESDOF. Obviously, if $P_{stripe} = 1.0$, the MDOF is essentially disregarded since it cannot be used for updating neither collapse or non-collapse SPO/ESDOF results. It can only provide some limited value, e.g., within an appropriate MLE refitting of the collapse fragility, if the SPO/ESDOF predicts a non-unitary collapse probability at the IM_{stripe} level.

Regarding the non-collapse data, the power-law model of Eq. (2) is regressed on the non-collapse data of SPO/ESDOF to estimate the a_{ESDOF}, b_{ESDOF}, and $\sigma_{\ln\varepsilon\text{-}ESDOF}$ parameters. If few or no collapses appear in the MDOF model, i.e., $P_{stripe} \leq 0.16$, then the analysis results of the MDOF are used to refine the a estimate of the power-law model, thus a_{ESDOF} is substituted by a_{MDOF} while the other two parameters are maintained constant. This is equivalent to shifting the linear fit of Eq. (2) in log-log space to match the median value implied by the MDOF while keeping the same intercept and variability. Consequently, the 3 parameters that describe the power-law-based approximation of the mixed model are a_{MDOF}, b_{ESDOF}, and $\sigma_{\ln\varepsilon-ESDOF}$. On the contrary, if more than 16% of collapses appear in the MDOF model, then the parameters of the power-law approximation are directly derived from SPO/ESDOF, thus being a_{ESDOF}, b_{ESDOF}, and $\sigma_{\ln\varepsilon-ESDOF}$.

Regarding collapse fragility, if no collapses appear in the MDOF stripe, the collapse fragility curve of the mixed model is directly obtained from the SPO/ESDOF. If, instead, MDOF collapse data is available, the point-estimate of the collapse probability, i.e., P_{stripe}–IM_{stripe}, can be used to refine the collapse fragility curve obtained from SPO/ESDOF. If, say, $0.20 \leq P_{stripe} \leq 0.80$ then the median value of the collapse fragility can be modified so that the fragility curve passes from the point estimate, while maintaining the same dispersion, β, as schematically presented in **Fig. 13**a. The median value of the modified distribution, $IM_{50,m}$, can be computed as:

$$\ln IM_{50,m} = \ln IM_{stripe} - \Phi^{-1}\left(P_{stripe}\right) \cdot \beta \tag{8}$$

where $\Phi^{-1}(\cdot)$ is the inverse of the standard normal cumulative distribution function. Obviously, the further away the point estimate is from the median (e.g. $P_{stripe} < 0.2$ or $P_{stripe} > 0.8$), the more haphazard such an approach becomes, as a tail-point would be used to bias correct a central value. In such cases, using the stripe information to bias correct the variability may become a more prudent choice, essentially rotating the initial lognormal curve around its median, IM_{50}, as shown in **Fig. 13**b. The modified dispersion, β_m, of the lognormal fragility curve in this case can be computed as:

$$\beta_m = \frac{\ln IM_{stripe} - \ln IM_{50}}{\Phi^{-1}\left(P_{stripe}\right)} \tag{9}$$

For the case-study building, the stripe analysis is performed on the MDOF model at the IM level with 10% probability of exceedance in 50 years, estimated at 0.62g via site-specific seismic hazard analysis. The 7 ground motion records that are used for the analyses are randomly selected from the FEMA P695 far-field ground motion set. The obtained $EDP\,|\,IM$ response of the MDOF model is presented in **Fig. 14**a. To allow fitting Eq. (2) and (3) the IDA analysis results of the ESDOF model are interpolated to produce multiple stripes of 44 points each, as shown in **Fig. 14**a where light grey color is used for the non-collapse points of stripes having more than 16% collapses and dark grey color for the lower ones.

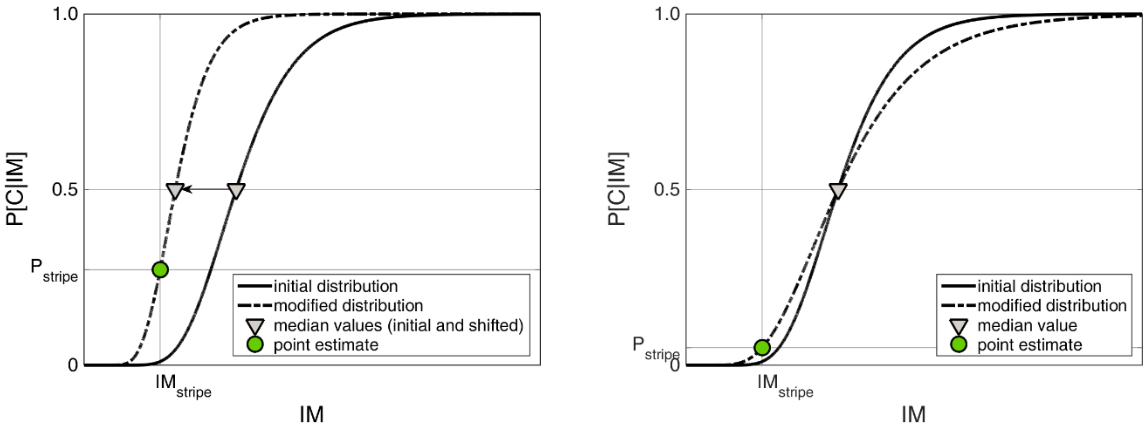

(a) updating the median (b) updating the dispersion

Fig. 13 Two options for updating the probability of collapse of the SPO/ESDOF approach to match the point estimate of the MDOF stripe: (a) The median of the lognormal fragility curve (grey triangle) is shifted to allow matching the point estimate (green bullet point) while the dispersion is kept constant, or (b) the dispersion of the lognormal fragility curve is modified to allow matching the point estimate (green bullet point) while the median value (grey triangle) is kept constant.

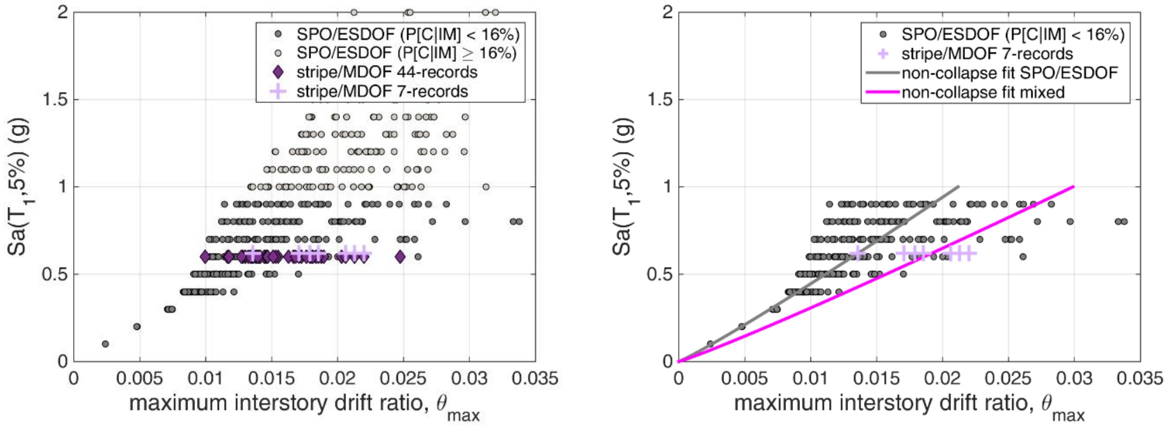

(a) non-collapse points from the stripe analyses of the SPO/ESDOF and the MDOF.

(b) power-law fit of the SPO/ESDOF and mixed models

Fig. 14 (a) Stripe analysis results of the SPO/ESDOF and the MDOF models and (b) power-law fit on the non-collapse data. The stripe analysis results shown by the rhombi and the crosses are performed at the same IM level, but they appear shifted for illustrative purposes.

The power-law based approximation is fitted on the stripes of the SPO/ESDOF model with less than 16% collapses, i.e., $P[C\,|\,IM] < 0.16$, to derive the pure pushover-based approximation, and then shifted to the right to predict higher EDP responses for any given IM per the MDOF stripe results, as a_{ESDOF} is substituted by a_{MDOF} to determine the mixed power-law fit of the non-collapse data (**Fig. 14**b). Since collapse data is not available in the MDOF stripe, the collapse fragility curve is directly derived from the SPO/ESDOF.

The fragility curves resulting from fitting the 5-parameter model on the SPO/ESDOF stripe results are presented in **Fig. 15**a–c for three indicative limit states defined at $\theta_{\max,C}$ = 0.01, 0.02 and 0.03. Note that the estimated ESDOF response distribution is practically identical to the predictions of the Ruiz-Garcia and Miranda (2007) relationships. In other words, we could achieve similar results by recreating stripes via sampling the distributions of response implied from published R-μ-T relationships, rather than performing IDA of the ESDOF system. The fragility curves of the mixed 5-parmeter surrogate as well as the lognormally fitted fragility curves computed by the full IDA results are also presented for both SPO/ESDOF and MDOF; obviously, running IDA on the latter is not required by the aforementioned procedure, only done for comparing. In all cases, the median and dispersion parameters of the lognormal fit of the fragilities are reported in **Table 3**.

First of all, to understand the limitations of the 5-parameter surrogate we should critically evaluate its fitting of the SPO/ESDOF results (denoted as SPO/ESDOF 5-parameter fit) against the underlying data (denoted as SPO/ESDOF IDA). As **Fig. 15**a–c show, these are fairly close at lower intensities but not as well matched higher up. Still, a fair matching can be claimed if one considers the simplification involved with using only 5 parameters. A better matching can be achieved if a more flexible parametric form is fitted, such as a smoothing spline or an elaborated fitted expression, but this is outside our present scope. Overall, though, this inability of the 5-parameter model to "perfectly" capture the underlying data is expected to propagate itself to the mixed-model results.

When pitting the SPO/ESDOF against the MDOF IDAs, it becomes clear that the fragilities of the former appear on the right of the MDOF fragilities, indicating an underestimation of response, as the ESDOF is clearly introducing bias in the assessment. Attempting to remove this bias via the model mixing comes with, admittedly, mixed results when only 7 records are employed. The 5-parameter surrogate does indeed shift the actual SPO/ESDOF fragility curves to the left, but it tends to overcorrect as the median of the 7 records led it slightly astray. Still, it can be claimed that it adequately corrects the bias for $\theta_{\mathrm{max},C}$ = 0.01 and 0.03, but not as well for $\theta_{max,C}$ = 0.02. Given the low number of records, there is some non-negligible sensitivity to the actual records selected for the MDOF stripe, here manifesting itself as an overcorrection of all fragility medians, and in other cases as undercorrection. When 44 records (or in general more than the minimalistic 7) are used in the stripe (see the 44 rhombi versus 7 crosses in **Fig. 14**a–b), the resulting fragility curves of the mixed model are closer to the ones computed from IDA on the MDOF model, thus offering an improved estimate of the structure's behavior.

Additional inherent limitations lie within this approach: Shooting for EDP_C values outside the EDP range obtained from the MDOF stripe, where not enough data is available, requires extrapolating the data and potentially increases the error. Nevertheless, data sparsity is a problem of its own and cannot be magically solved by a surrogate. Given the initial conditions and the limited data at hand, it is hard to argue that a better fragility estimate can be found without adding more MDOF dynamic analyses.

Table 3 Fragility curve median and dispersion values, in terms of $Sa(T_1,5\%)$ assuming lognormality, for all approaches and limit states.

Approach / Limit State	**MDOF 44 records IDA**	**SPO/ESDOF 44 records IDA**	**SPO/ESDOF 44 records (5-param model fit)**	**Mixed 7-record MDOF stripe**	**Mixed 44-record MDOF stripe**
$\theta_{max,C}$ = 1.0%	0.38 (18%)	0.43 (12%)	0.45 (19%)	0.31 (19%)	0.38 (19%)
$\theta_{max,C}$ = 2.0%	0.84 (25%)	0.97 (30%)	0.90 (19%)	0.64 (18%)	0.79 (18%)
$\theta_{max,C}$ = 3.0%	1.07 (27%)	1.29 (33%)	1.21 (25%)	0.95 (19%)	1.11 (22%)

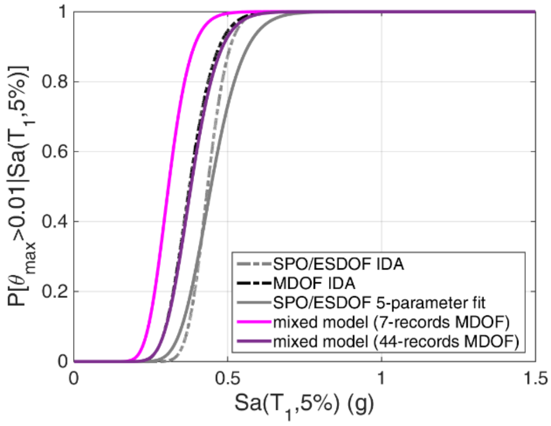

(a) fragility curves for $\theta_{max,C}$ = 1.0%

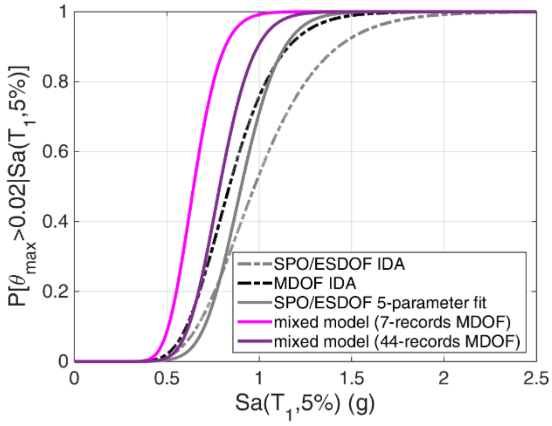

(b) fragility curves for $\theta_{max,C}$ = 2.0%

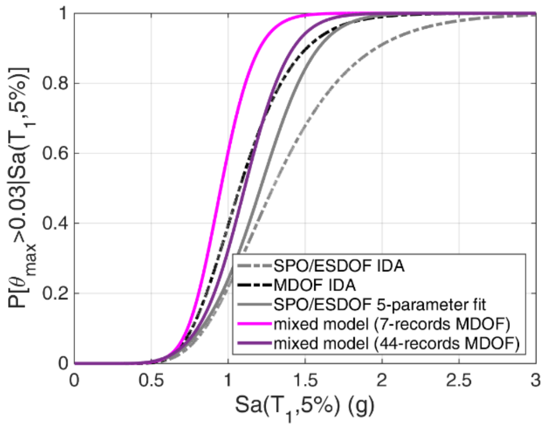

(c) fragility curves for $\theta_{max,C}$ = 3.0%

Fig. 15 Fragility curves for all examined limit states.

5 Conclusions

Mixed probabilistic demand models can combine different analysis options of multiple fidelities into a single surrogate that is suitable for fragility assessment. The examples shown use as a vehicle the 5-parameter power-law-based surrogate and they enable us to obtain reliable estimates of the fragility curves even in regions where inadequate data is available. When it comes to combining structural models of different fidelities, the selection of relative weights depends on the user's own preferences and beliefs about the validity of each model in each region: By modifying the relative weights, the mixed probabilistic seismic demand model is capable of capturing the response of each single source model and any combination in between. In contrast, when mixing different analysis methods, there is an undeniable superiority of the nonlinear dynamic versus the nonlinear static results. Still, the 5-parameter surrogate can be employed to update the full-range static pushover results via a single sparse stripe analysis of the MDOF model. The value of this approach becomes more apparent when considering highly complex models where each response history analysis comes at a considerable cost, and taking advantage of every single point estimate available is of paramount importance. All in all, it can be claimed that the mixing of two or more seismic-demand models even via simplified surrogates is a useful tool, yielding results that are much more than a sum of their parts.

6 Acknowledgements

Financial support has been provided by the Eugenides Foundation in Greece (scholarship for doctoral studies in NTUA grant) and by the Innovation and Networks Executive Agency (INEA) under the powers delegated by the European Commission through the Horizon 2020 program “PANOPTIS-development of a decision support system for increasing the resilience of transportation infrastructure based on combined use of terrestrial and airborne sensors and advanced modelling tools”, Grant Agreement number 769129.

7 Declarations

Funding

EU Horizon2020, Grant Agreement number 769129

Eugenides Foundation, Doctoral Grant Scholarship 2018

Conflicts of interest/Competing interests

The authors have no conflicts of interest to declare that are relevant to the content of this article.

Availability of data and material

The stripe analysis results of both Applications are available on GitHub: https://github.com/TheLambdaLab/MixedModels_paper.git, while the 2D models of the 4-story MRF are available at http://users.ntua.gr/divamva/RCbook.html

Code availability

The code needed to replicate Applications 1 and 2 is available on GitHub: https://github.com/TheLambdaLab/MixedModels_paper.git.

Authors' contributions:

A. Chatzidaki: Formal analysis and investigation; Methodology; Writing - original draft preparation.

D. Vamvatsikos: Conceptualization, Supervision, Writing - review and editing.

8 References

ASCE 41-13 (2014). Seismic evaluation and retrofit of existing buildings. American Society of Civil Engineers, Reston, VA

Aschheim M, Hernández-Montes E, Vamvatsikos D (2019). Design of reinforced concrete buildings for seismic performance: practical, deterministic and probabilistic approaches, CRC Press

Baker JW (2015). Efficient analytical fragility function fitting using dynamic structural analysis. Earthq Spec 31(1): 579-599. https://www.doi.org/10.1193/021113EQS025M

Baltzopoulos G, Baraschino R, Iervolino I, Vamvatsikos D (2017). SPO2FRAG: software for seismic fragility assessment based on static pushover. Bull Earthq Eng 15(10): 4399-4425. https://doi.org/10.1007/s10518-017-0145-3

Baltzopoulos G, Baraschino R, Iervolino I, Vamvatsikos D (2018). Dynamic analysis of single-degree-of-freedom systems (DYANAS): a graphical user interface for OpenSees. Engin Struct 177: 395-408. https://www.doi.org/10.1016/j.engstruct.2018.09.078

Baltzopoulos G, Vamvatsikos D, Iervolino I (2016). Analytical modelling of near-source pulse-like seismic demand for multi-linear backbone oscillators. Earthq Eng Struct Dyn, 45(11): 1797-1815. https://doi.org/10.1002/eqe.2729

Chatzidaki A, Vamvatsikos D (2021) Reinforced concrete building seismic design examples (available at http://users.ntua.gr/divamva/RCbook.html)

Chi W, El-Tawil S, Deierlein GG, Abel JF (1998). Inelastic analyses of a 17 story framed building damaged during Northridge. Eng Struct 20(4-6): 481-495. https://doi.org/10.1016/S0141-0296(97)00036-9

Cornell CA, Krawinkler H (2000). Progress and challenges in seismic performance assessment, PEER Center News 2000, 3(2): 1-4. https://apps.peer.berkeley.edu/news/2000spring/performance.html (Dec. 12, 2020).

De Luca F, Vamvatsikos D, Iervolino I (2013). Near-optimal piecewise linear fits of static pushover capacity curves for equivalent SDOF analysis. Earthq Eng Struct Dyn, 42(4): 523-543. https://www.doi.org/10.1002/eqe.2225

Elkady A, Lignos D (2018). II-DAP: interactive interface for dynamic analysis procedures (Version 1.1). Zenodo. http://doi.org/10.5281/zenodo.1480341

Elnashai AS (2001). Advanced inelastic static (pushover) analysis for earthquake applications. Struct Eng Mechanics, 12(1): 51-69. http://doi.org/10.12989/sem.2001.12.1.051

EN1998-3 (2005). Eurocode 8: Design of structures for earthquake resistance - Part 3: Assessment and retrofitting of buildings. European Committee for Standardization, Brussels

Fajfar P (2000). A nonlinear analysis method for performance-based seismic design. Earthq Spec 16(3): 573-592. https://www.doi.org/10.1193/1.1586128

FEMA (2009). FEMA P695 Far field ground motion set. Available at: http://users.ntua.gr/divamva/RCbook/FEMA-P695-FFset.zip (Accessed 27/01/2019)

Fernández-Godino MG, Park C, Kim NH, Haftka RT (2019). Issues in deciding whether to use multifidelity surrogates. AIAA J. https://doi.org/10.2514/1.J057750

Fragiadakis M, Vamvatsikos D, Aschheim M (2014). Application of nonlinear static procedures for seismic assessment of regular RC moment frame buildings. Earthq Spectra 30(2):767-794.

Haselton CB, (2008). Assessing seismic collapse safety of modern reinforced concrete moment frame buildings. Ph.D. Dissertation, Stanford, CA.

Haselton CB, Liel AB, Dean BS, Chou JH, Deierlein GG (2007). Seismic collapse safety and behavior of modern reinforced concrete moment frame buildings. Res Front Struct Cong. https://doi.org/10.1061/40944(249)22

Hastie T, Tibshirani R, Friedman J (2009). The elements of statistical learning: data mining, inference, and prediction. Springer.

Ibarra L, Krawinkler H (2011). Variance of collapse capacity of SDOF systems under earthquake excitations. Earthq Eng Struct Dyn 40(12): 1299-1314. https://doi.org/10.1002/eqe.1089

Jalayer F (2003). Direct probabilistic seismic analysis: implementing nonlinear dynamic assessments. Ph.D. Thesis, Dept of Civil and Environmental Engineering, Stanford: Stanford University

Jalayer F, Cornell CA (2009). Alternative non-linear demand estimation methods for probability-based seismic assessments. Earthq Eng Struct Dyn 38(8): 951-972. https://doi.org/10.1002/eqe.876

Jalayer F, De Risi R, Manfredi G (2015). Bayesian cloud analysis: efficient structural fragility assessment using linear regression. Bull Earthq Eng 13: 1183-1203. https://doi.org/10.1007/s10518-014-9692-z

Jalayer F, Elefante L, Iervolino I, Manfredi G (2011). Knowledge-based performance assessment of existing RC buildings. J Earthq Eng 15(3): 362-389. https://doi.org/10.1080/13632469.2010.501193

Jalayer F, Iervolino I, Manfredi G (2010). Structural modeling uncertainties and their influence on seismic assessment of existing RC structures. Struct Saf 32(3): 220-228. https://doi.org/10.1016/j.strusafe.2010.02.004

Kazantzi AK, Vamvatsikos D, Lignos DG (2014). Seismic performance of a steel moment-resisting frame subject to strength and ductility uncertainty. Eng Struct 78: 69-77. https://doi.org/10.1016/j.engstruct.2014.06.044

Kohrangi M, Bazzurro P, Vamvatsikos D, Spillatura A (2017). Conditional spectrum-based ground motion record selection using average spectral acceleration. Earthq Eng Struct Dyn 46(10): 1667-1685. https://doi.org/10.1002/eqe.2876

Krawinkler H, Seneviratna GDPK (1998). Pros and cons of a pushover analysis of seismic performance evaluation. Eng Struct 20(4-6): 452-464. https://doi.org/10.1016/S0141-0296(97)00092-8

Lachanas C, Vamvatsikos D (2020). Model type effects on the estimated seismic response of a 20-story steel moment resisting frame. J Struct Eng 147(6). https://doi.org/10.1061/(ASCE)ST.1943-541X.0003010

Lin T, Harmsen SC, Baker JW, Luco N (2013a). Conditional spectrum computation incorporating multiple causal earthquakes and ground-motion prediction models. Bull Seismolog Society Am 103(2A): 1103-1116. https://doi.org/10.1785/0120110293

Lin T, Haselton CB, Baker JW (2013b). Conditional spectrum-based ground motion selection. Part I: Hazard consistency for risk-based assessments. Earthq Eng Struct Dyn. 42(12): 1847-1865. https://doi.org/10.1002/eqe.2301

Mander JB, Priestley MJN, Park R (1988). Theoretical stress-strain model for confined concrete. J Struct Eng 114(8): 1804-1826. https://doi.org/10.1061/(ASCE)0733-9445(1988)114:8(1804)

Mazzoni S, McKenna F, Scott M and Fenves G (2000). Open system for earthquake engineering simulation: OpenSees command language manual, University of California, Berkeley, CA. http://opensees.berkeley.edu/

Miranda E (2001). Estimation of inelastic deformation demands of SDOF systems. J Struct Eng, 127(9): 1005-1012. https://doi.org/10.1061/(ASCE)0733-9445(2001)127:9(1005)

Parr WC (1981). Minimum distance estimation: a bibliography. Commun Stat Theory Methods 10(12): 1205-1224. https://doi.org/10.1080/03610928108828104

Patsialis D, Taflanidis AA (2020). Multi-fidelity Monte Carlo for seismic risk assessment applications. Struct Saf (in review).

Peherstorfer B, Willcox K, Gunzburger M (2018). Survey of multifidelity methods in uncertainty propagation, inference, and optimization. Siam Review 60(3): 550-591. https://doi.org/10.1137/16M1082469

Ruiz-García J, Miranda E (2007). Probabilistic estimation of maximum inelastic displacement demands for performance-based design. Earthq Eng Struct Dyn 36(9): 1235-1254. https://doi.org/10.1002/eqe.680

Shome N, Cornell CA. (1999). Probabilistic seismic demand analysis of nonlinear structures. Report No. RMS-35, RMS Program, Stanford University, Stanford, CA.

Silva V, Akkar S, Baker JW, Bazzurro P, Castro JM, Crowley H, Dolsek M, Galasso C, Lagomarsino S, Monteiro R, Perrone D, Pitilakis K, Vamvatsikos D (2019). Current challenges and future trends in analytical fragility and vulnerability modelling. Earthq Spec 35(4): 1927-1952. https://doi.org/10.1193/042418EQS101O

Sousa R, Almeida JP, Correia AA, Pinho R (2020). Shake table blind prediction tests: contributions for improved fiber-based frame modelling. J Earthq Eng 24(9): 1435-1476. https://doi.org/10.1080/13632469.2018.1466743

Tsioulou A, Galasso C (2018). Information theory measures for the engineering validation of ground-motion simulations. Earthq Eng Struct Dyn 47(4): 1095-1104. https://doi.org/10.1002/eqe.3015

Vamvatsikos D, Aschheim M (2016). Performance-based seismic design via yield frequency spectra. Earthq Eng Struct Dyn 45(11): 1759-1778. https://doi.org/10.1002/eqe.2727

Vamvatsikos D, Cornell CA (2002). Incremental dynamic analysis. Earthq Eng Struct Dyn 31(3): 491-514. https://doi.org/10.1002/eqe.141

Vamvatsikos D, Cornell CA (2006). Direct estimation of the seismic demand and capacity of oscillators with multi-linear static pushovers through IDA. Earthq Eng Struct Dyn 35(9): 1097-1117. https://doi.org/10.1002/eqe.573

Vamvatsikos D, Fragiadakis M (2010). Incremental dynamic analysis for estimating seismic performance sensitivity and uncertainty. Earthq Eng Struct Dyn 39(2): 141-163. https://doi.org/10.1002/eqe.935

Weisberg S (2005). Applied linear regression (Vol. 528). John Wiley & Sons.